I212T001008.212
T001008d.212

The Global Atmosphere and Ocean System, 2000, Vol. 00, pp. 1–25
Reprints available directly from the publisher
Photocopying permitted by license only

QUASISYNCHRONOUS OBSERVATIONS OF THE GULF STREAM FRONTAL ZONE WITH ALMAZ-1 SAR AND MEASUREMENTS TAKEN ON BOARD THE R/V AKADEMIK VERNADSKY

SEMYON GRODSKY[a,*], VLADIMIR KUDRYAVTSEV[a] and ANDREY IVANOV[b]

[a]*Marine Hydrophysical Institute, Ukrainian Academy of Science, 2, Kapitanskaya str., Sevastopol, 335000, Ukraine;* [b]*P.P. Shirshov Institute of Oceanology, 36 Nakhimovsky Pr., Moscow 177851, Russia*

(Received in final form 1 September 2000)

Quasisynchronous observations of the Gulf Stream frontal zone with ALMAZ-1 Synthetic Aperture Radar (SAR) and concurrent measurements taken on board the R/V AKADEMIK VERNADSKY are analyzed. Sea surface temperature fields from NOAA satellites are additionally used. Space imaging was accompanied by measurement of the standard hydrologic and meteorological parameters, and registration of surface currents along the route of the vessel crossing the frontal zone. Comparison of satellite and *in-situ* wave measurements has shown that ALMAZ-1 SAR displays the basic parameters of long waves (wavelength and orientation) rather precisely. Based on 2-D radar image spectra the effects of wave refraction are investigated. The surveys were carried out at moderate westerly winds when the waves evolved in the along current direction. In these conditions, the effects of wave reflection produced the zones of wave concentration and wave "shadow". Based on synchronous satellite and *in-situ* measurements, the wave-radar image modulation transfer function (MTF) were estimated and used to retrieve wave elevation variance from radar image spectra. The estimations of wave energy changes corresponded qualitatively to spatial variations in the ship vertical displacement variance. Linear features oriented along the Gulf Stream were revealed in SAR images. They originate from wave-current interaction and short wave damping in areas of sargassum accumulations (convergence).

Keywords: Wave; SAR; Wave refraction; The gulf stream signature

*Address for correspondence: Department of Meteorology, University of Maryland, Computer and Space Science Bldg. #4335, College Park, MD 20742. e-mail: senya @ ocean2.umd.edu

1. INTRODUCTION

Ocean mesoscale fronts, are areas of intensive energy and substance exchange between ocean and atmosphere, influence on biological processes, and have appreciable signatures on the sea surface. The ability of observing them by spaceborn Synthetic Aperture Radar (SAR), possessing high spatial resolution, was shown for the first time with SEASAT SAR (see for example, Beal *et al.*, 1981). These observations and later ones carried out with ERS-1 SAR (Johannessen *et al.*, 1994; Nilsson *et al.*, 1995; Beal *et al.*, 1997) and KOSMOS-1500 RAR (Mitnik *et al.*, 1989) have shown that these radars provide an opportunity to investigate thermal structure of the frontal zones and detect current boundaries.

Current variations across the frontal zones may influence surface waves significantly. Theory predicts (see *e.g.*, Kenyon, 1971) the most interesting effects: wave reflection by a current and waveguide-like propagation of the trapped wave towards the current. Trapped wave concentration in a jet can cause a danger to navigation (Gutshabash and Lavrenov, 1986). Wave-current interaction forces spatial variation of wave energy. This was explicitly shown by Liu *et al.* (1994) from empirical analysis of wave ray refraction patterns inferred from ERS-1 SAR image received over an oceanic eddy and model calculations.

Spaceborn SAR resolves long surface waves allowing investigation of wave refraction on current inhomogeneuties (Barnett *et al.*, 1989; Sheres *et al.*, 1985). Wave evolution on the Gulf Stream and wave refraction on a warm core ring were observed by SEASAT SAR (Beal *et al.*, 1986; Mapp *et al.*, 1983). The SIR-B data were used to research the trapped waves in the Agulhas current (Irvine and Tilley, 1988), and wave behavior in the Circumpolar area (Barnett *et al.*, 1989). However, these data were not supported by synchronous measurements of currents.

One of the most complete observations of wave evolution was performed by Kudryavtsev *et al.* (1995) on board the R/V AKADEMIK VERNADSKY, which crossed the Gulf Stream frontal zone repeatedly in August–September 1991. In this experiment radar wave observations, accompanied by registration of surface currents and the Marine Atmospheric Boundary Layer parameters, have been performed in conditions, which allowed the most prominent peculiarities of wave-current interaction, including wave reflection by current and wave trapping by opposing jet to be revealed. Shipboard measurements were supplemented by quasisynchronous satellite ALMAZ-1 SAR imaging of the experimental area.

This paper is aimed at the analysis of the Gulf Stream radar signatures and wave behavior on a shear current based on the ALMAZ-1 SAR data and the R/V AKADEMIK VERNADSKY measurements. Experiments were performed at the end of August and beginning of September 1991 as a part of the OKEAN-I field program (Viter *et al.*, 1993).

2. GENERAL DESCRIPTION OF THE EXPERIMENT

The Gulf Stream radar surveys were carried out on August 23, 28, 29 and on September 7, 8, 1991. The study is limited to analysis of data collected on August 28, 29 and September 7. These days the surface waves were high enough to be resolved by a SAR, and *in-situ* ship measurements were collected. The experiments were performed under westerly wind with speed $5\,\mathrm{m/s} < W < 15\,\mathrm{m/s}$.

The Gulf Stream temperature front position was determined from AVHRR NOAA data received by ship station (the Automatic Picture Transmission Regime). The surface measurements were carried out from a moving vessel, which crossed the current in a direction perpendicular to the front with measurements of the oceanic and atmospheric boundary layer parameters along a route located within an image swath. *In-situ* wave records were carried out on August 28 and September 7 at the time of satellite overpass by a one-component drifting buoy accelerometer. A ship measuring complex described by Kudryavtsev *et al.* (1995) allowed registration of: sea surface temperature, T_w, air temperature, T_a, wind velocity, **W**, surface current, U, whitecap coverage, Q, vertical displacement of the vessel (when moving) and wave vertical acceleration (when the vessel was drifting). The current speed was registered by the towed Electromagnetic Kinetograph (EK), which measures flow component perpendicular to ship heading. To estimate surface current, U, the assumption that the Gulf Stream is a flat parallel jet directed along the T_w front was used.

Radar surveys were planned so that the images covered both northern and southern sides of current. It has allowed analysis of a radar fingerprint of the Gulf Stream front and investigation of spatial non-homogeneity of waves caused by their interaction with the current.

Table I presents the parameters of images collected by ALMAZ-1 SAR during the experiment.

TABLE I List of ALMAZ-1 SAR images and the parameters of environmental conditions

Date, 1991	*August* 28	*August* 29	*September* 7
Orbit	2396 *a*	2418 *d*	2560 *a*
Time, UTC	12 : 16	21 : 45	19 : 32
Distance R, km	340	330	370
Incident angle, deg	29	29	33
Image dimension, km	58.1 × 215.3	63.2 × 97.8	54.6 × 217.2
Wind (at the moment of imaging):			
speed, m/s	10	8	12
azimuth (from), deg	260	280	290
Wave information			
wavelength, m	150; 150	150; 80 ÷ 110	140 ÷ 150
azimuth, deg	20 ÷ 50; 80 ÷ 90	135; 80 ÷ 110	130 ÷ 140
wave displacement variance, m^2	–	0.26	0.58

3. CHARACTERISTICS OF ALMAZ-1 SAR AND DATA PROCESSING PROCEDURE

The main parameters of ALMAZ-1 SAR are summarized by Alpers *et al.* (1994) and briefly in Table II.

SAR spatial resolution allows observation of long surface waves. To investigate them, 2-D radar image spectra were calculated. Each spectrum represents the squared modulus of the FFT transform of radiance distribution within an elementary 128×128 points image subscene (pixel size 10×10 m). Final spectral estimates were smoothed over a frame containing $7 \times 7 = 49$ elementary subscenes (frame size 9×9 km) with the subsequent smoothing on squares 3×3 in **k**-space, that provided ~ 900 degrees of freedom.

The image spectrum is related to wave one by the spatial wave-radar Modulation Transfer Function (MTF), which is not known *a priori*. It consists of three basic terms (Alpers *et al.*, 1981): geometrical, Mt, hydrodynamic, Mh, and an additional term due to velocity bunching effect, Mv. The last one is the most interesting from the viewpoint of SAR imaging.

TABLE II Parameters of ALMAZ-1 SAR

Active period	91.03.31 – 92.10.17
Orbit altitude	270 ÷ 380 km
Orbit inclination	72.7°
Wavelength	9.6 cm
Ground resolution	10 ÷ 15 m
Incidence angle	varying, 25° ÷ 60°
Swath width at different incidence angles	35 ÷ 55 km
Polarization	horizontal (HH)
SAR integration time	0.3 s

It is caused by azimuthal displacement Δx in the image plane of a moving target, which is proportional to a projection of its speed to inclined range $\Delta x = (R/V)v_R$, where V is the satellite ground velocity. At $v_R \sim 1$ m/s the value $\Delta x \sim 45$ m is comparable to the length of a registered wave λ. If the wavelength projection on the direction of flight $\lambda_x < \lambda^+ = 4\Delta x$, the wave imaging is essentially nonlinear. An estimation of λ^+ for ALMAZ-1 SAR equals $\lambda^+ \approx 100$ m at a wave steepness of $\varepsilon = 0.05$.

The velocity bunching mechanism allows imaging of azimuth wave component restricting (at the same time) SAR resolution in the flight direction. According to Hassellmann *et al.* (1985), the total MSR displacement, δx, of the image is formed by: (1) statistical contribution of the orbital velocities of intermediate scale waves within SAR resolution cell, δx_i, (2) time changes (within integration interval) in orbital velocities of waves resolved by SAR, δx_l. They can be estimated as:

$$\delta x_i = \frac{R}{V}\cos\theta\sqrt{\frac{g\alpha}{2k_{\mathrm{SAR}}}} \quad \delta x_l = \frac{R}{V}\cos\theta g T_i\sqrt{\frac{\alpha}{24}\ln\frac{k_{\mathrm{SAR}}}{k_p}}, \tag{1}$$

where $k_{\mathrm{SAR}} = 2\pi/10$, m^{-1} is the wavenumber determined by the SAR resolution scale, k_p is the spectrum peak wavenumber, $\alpha = 0.01$. At $V = 7.5$ km/s, $R/V = 45$, $k_p = 0.1$ rad/m, Eq. (1) yields $\delta x_i \approx 13$ m, $\delta x_l \approx 4$ m and $\delta x = (\delta x_i^2 + \delta x_l^2)^{0.5} \approx 14$ m. Spatial size of an averaging element is limited on a 95% confidence level by an interval $\pm 2\delta x$, hence the waves with azimuth wavenumber $k_x 2\delta x > \pi (k_x > k_a \approx 2\pi/50\,\mathrm{rad/m})$ are not resolved by the radar.

Figure 1a shows an example of an initial radar image spectrum $S_\sigma^{(0)}(k_y, k_x)$ and indicates non-zero energy level at $k_x > k_a$ which is caused by noise. The SAR image speckle forms broadband (''white''-like) noise in a wavenumber range $k < k_{\mathrm{SAR}}$ (Hassellmann *et al.*, 1985). If the synthesis is carried out along both coordinates, the noise will be two-dimensional ''white''. In ALMAZ-1 SAR the synthesis was carried out only in the flight direction, thus the spectrum of noise S_n is broadband only in azimuth direction and depends on the radial wavenumber $S_n = S_n(k_y)$. Figure 1b presents the spectrum shown in Figure 1a after correction with a stationary response function accounting for the finite spatial resolution of the system: $S_\sigma^{(1)}(k_y, k_x) = S_\sigma^{(0)}(k_y, k_x)/\mathrm{SIRF}^2(k_y, k_x)$. The shape of the $\mathrm{SIRF}^2(k_y, k_x)$ function for ALMAZ-1 SAR is presented in (Wilde *et al.*, 1993). After correction, the isolines of the high-frequency part of the spectrum became mostly parallel to the vertical axis (direction of flight) that confirms functional dependence of a noise spectrum only on k_y. In Figure 1c the

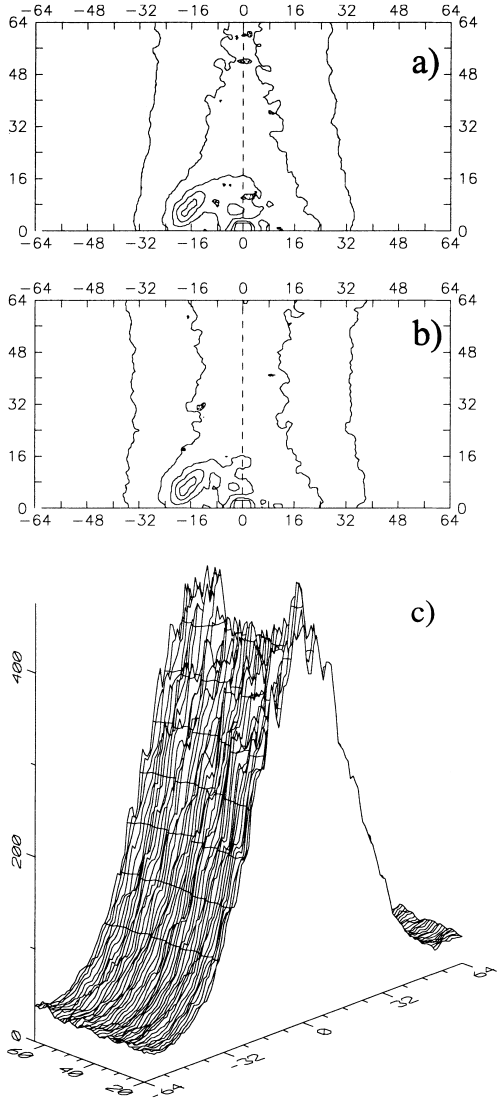

FIGURE 1 (a) An example of 2-D radar image spectrum. The vertical axis is oriented in the flight direction. Isolines are drawn in 0.2 $S_{\max}$ (where $S_{\max}$ – is the spectrum peak level) starting with 0.1 $S_{\max}$. Discreteness in wave number is 0.005 rad/m. (b) The same spectrum after correction on the SAR stationary response function. (c) The high-frequency portion of the spectrum shown in frame (b). The vertical axis presents relative level of energy; 1000 corresponds to $S_{\max}$.

perspective view of the high-frequency part of $S_{\sigma}^{(1)}(k_y, k_x)$ is shown, the spectrum shape is close to cylindrical one with an axis parallel to flight direction. It allows to estimate the noise spectrum as:

$$S_n(k_y) = \frac{\int_{k_x > k_a} S_\sigma^{(1)}(\mathbf{k}) dk_x}{\int_{k_x > k_a} dk_x}, \tag{2}$$

where $k_a = 2\pi/50$ rad/m as estimated earlier. This will be further subtracted from the radar spectrum as:

$$S_\sigma(k_y, k_x) = \max(0, S_\sigma^{(1)}(k_y, k_x) - S_n(k_y)). \tag{3}$$

Alpers *et al.* (1994) have shown that due to smaller orbit height, ALMAZ-1 SAR displays sea waves more linearly than (for example) ERS-1 SAR, and its images are possible to use for analysis of the long sea waves. Tilley *et al.* (1994) comparison of ERS-1 and ALMAZ-1 estimates of directional ocean spectra confirmed that SAR imaging of ocean waves can be improved by flying platform with low range to velocity ratio, R/V, (like ALMAZ-1) by alleviating the azimuth smearing.

We shall note also, that ALMAZ-1 SAR worked in an automatic amplifier control mode, which damped "slow" changes of a signal. The time constant ~ 1.5 sec corresponds to filtering out the harmonics with spatial scales exceeding 10 km in the flight direction.

4. COMPARISON OF RADAR AND *IN-SITU* MEASUREMENTS OF WAVE SPECTRA

Synchronous with radar imaging *in-situ* wave records were obtained with a buoy accelerometer on August 29 and September 7. On August 29, wave measurements were taken at point E (see Fig. 5 below), and in the experiment September 7 – in a vicinity of point #12 (see Fig. 8). Figures 2a and 2b display wavenumber spectra $S(k)$ calculated from surface elevation frequency spectra using the deep-water linear wave dispersion relation. These spectra satisfy a condition $\int S(k)dk = \langle \zeta^2 \rangle$, where $\langle \zeta^2 \rangle$ is the wave elevation variance. Figure 2 also presents radar image omnidirectional spectra normalized by the square of an average radar signal: $S_\sigma(k)/\langle \sigma \rangle^2$. They are obtained by integration over azimuth φ of 2-D radar image spectra $S_\sigma(k) = \int S_\sigma(\mathbf{k}) k dk d\varphi$. Referring to Figures 2a and b, we find that the radar spectrum reproduces satisfactorily the spectral shape of the energy containing waves and the spectral peak position on the wavenumber axis.

Figure 2c illustrates the magnitude of wave-radar MTF $M(k)$, which relates omnidirectional radar image spectrum and *in-situ* wave spectrum:

$$M(k) = \sqrt{\frac{S_\sigma(k)}{\langle \sigma \rangle^2 k^2 S(k)}} \tag{4}$$

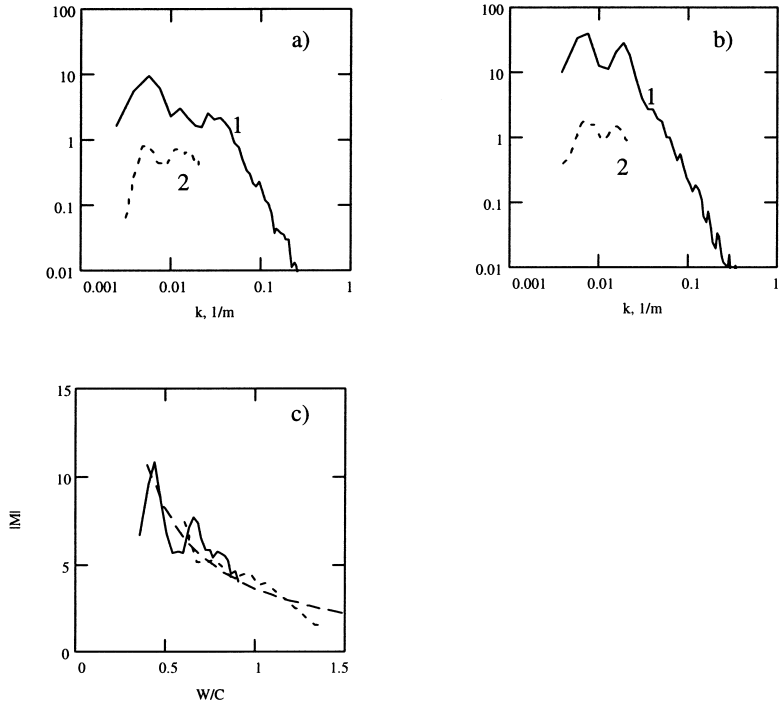

FIGURE 2 *In-situ* wave elevation spectra $S(k)$, m^3 (1) and omnidirectional radar image spectra $S_\sigma(k)/\langle 0\rangle^2$, normalized by the mean radar signal squared (2) taken on August 29 (a) and September 7 (b). (c) The wave-radar image MTF estimates for August 29 (solid line, $W=8$ m/s) and for September 7 (short dashed, $W=12$ m/s), and their best fit by power function of dimensionless wave frequency: $M(k)=3.6(W/C)^{1.18}$ (long dashed).

The MTF magnitude decreases with increasing dimensionless wave frequency W/C, where $C=(g/k)^{0.5}$ is the phase speed. The $M(k)$ approximation in terms of a power function of W/C is: $M=\exp(p_1)/(W/C)_2^p$, where $p_1=1.28\pm0.04$ and $p_2=1.18\pm0.1$. It will be used further for an estimation of wave elevation variance from SAR image spectra, namely $\langle\zeta^2\rangle_R=\int(S_\sigma(k)dk/\langle\sigma\rangle^2k^2M^2(k))$.

5. RADAR OBSERVATIONS OF WAVE SPECTRA EVOLUTION

We shall consider variability of waves in the Gulf Stream frontal zone on the basis of 2-D SAR spectra and wave ray calculation. A simple technique utilizing the wave ray approach is a valuable tool that provides an insight

into the physics of wave-current interaction and helps in understanding the wave variability in the areas of non-uniform currents (see *e.g.*, Vachon *et al.*, 1995). The accuracy of wave ray calculations is limited (as a rule) by an insufficient knowledge of the spatial picture of surface currents. Preliminary interpretation of the data presented in this paper as well as the analysis of sensitivity of the wave ray pattern to accuracy of the current field are presented in Grodskii *et al.* (1992, 1996a, b) and Grodsky *et al.* (1996c). It has been shown that the wave pattern is influenced sufficiently by the mutual orientation of waves and surface flow and by the value of maximal current speed. The direction of current is known indirectly through the SST front configuration. The crosscurrent speed profile comes from the only one section along the ship route. It is extrapolated assuming the flat parallel flow model following the shape of the SST front. Accounting for possible inaccuracy of the spatially extrapolated surface flow field, we shall further consider the results of wave ray calculations only as a proxy showing that the observed wave situations can potentially exist.

Experiment August 28 Figure 3 shows the scheme of the experiment as a Sea Surface Temperature (SST) map with SAR image (smoothed to 1 km resolution) overlaid. The Gulf Stream thermal front separates colder shelf waters (24°C, dark) and warm waters of the current (28° – 29°C, bright). The location of a zone of the maximum temperature gradients coincides rather precisely with a zone of maximum current speed. General parameters of this and other experiments are summarized in Table I.

The *in-situ* measurements were taken along a trajectory of the vessel crossing the current. At the moment of imaging the ship was at a point with coordinates 39.40 N, 63.60 W. According to visual observations from the ship, on the southern side of the Gulf Stream there was a mixed sea consisting of several wave systems traveling in a sector between the east and the north directions. On the northern side only one system of the NNE direction existed. It agrees with radar image subscenes (size 256 × 256 pixels, resolution 10 m) shown in the lower panel of Figure 3 and presenting an enhanced image structure at points #4 and #22. They were obtained by direct and inverse FFT calculations with eliminating of harmonics lying below 40% of the maximum energy level. The wave field south of the jet (point #22) consists of two systems, and on the northern side of the Gulf Stream (point #4) only one wave mode exists. The two systems have wavelength ~150 m, and their orientation is shown by arrows.

The spectra presented in Figure 3 illustrate the basic peculiarities of the wave field. It shows the essential changes of character of the waves on

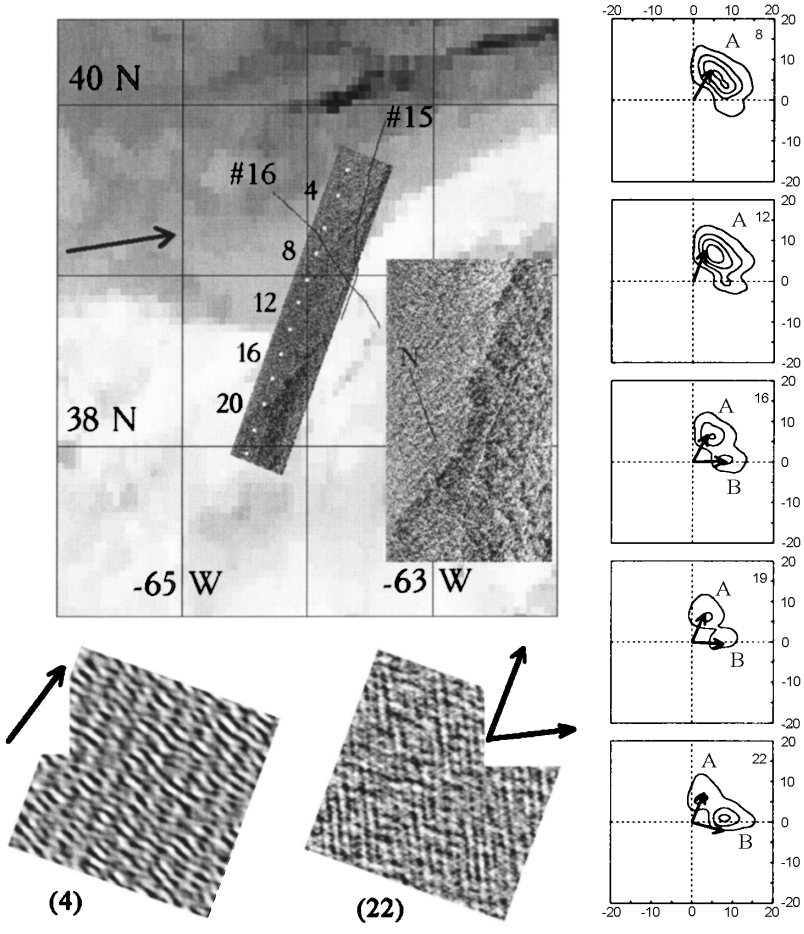

FIGURE 3 On the left. Scheme of Experiment August 28, 1991. ALMAZ-1 SAR image (#2396a, 12:16 GMT) inlaid in the AVHRR SST field (08:00 GMT). Also shown are the numbers and positions of image subscenes used to calculate radar image spectra, the wind direction, and the vessel routes. The following are presented in more details: the southern part of radar image, and the image subcsenes at points #4 and #22 with the wave systems direction shown by the arrows. On the right. The sample of 2-D radar spectra. Discreteness in wavenumber is 0.005 rad/m. Isolines are drawn in 20% of the maximum energy level of all spectra. The arrows show the wavenumbers corresponding to local maxima of model spectra calculated with adiabatic approximation.

the northern side of the Gulf Stream (points 8 . . . 12) in comparison to the southern one (points 16 . . . 22). Analyzing the spectral shape, one can select two wave systems. The spectral peaks corresponding to these wave systems are marked with symbols *A* and *B* in Figure 3 (right panel). On the northern side of the current (points 8 . . . 12), the radar spectra have a single peak

(system *A*). On its southern side (points 16...22), the spectrum's angular width increases due to the presence of two wave systems. At the same time, the spectra have higher energy level on the northern side of the Gulf Stream, which indicates wave concentration in this part of the current.

The local maximum *A* corresponds to waves crossing the current and is observed on all spectra. The maximum *B* is registered only on the southern side and can be explained as waves reflected by the Gulf Stream. This hypothesis is confirmed by a ray calculation performed for an uniform wave field south off the Gulf Stream with a wave vector corresponding to system *A* (see Fig. 4a). It shows that due to refraction the background wave field is separated into two systems, *A* and *B*, depending on the local incidence angle.

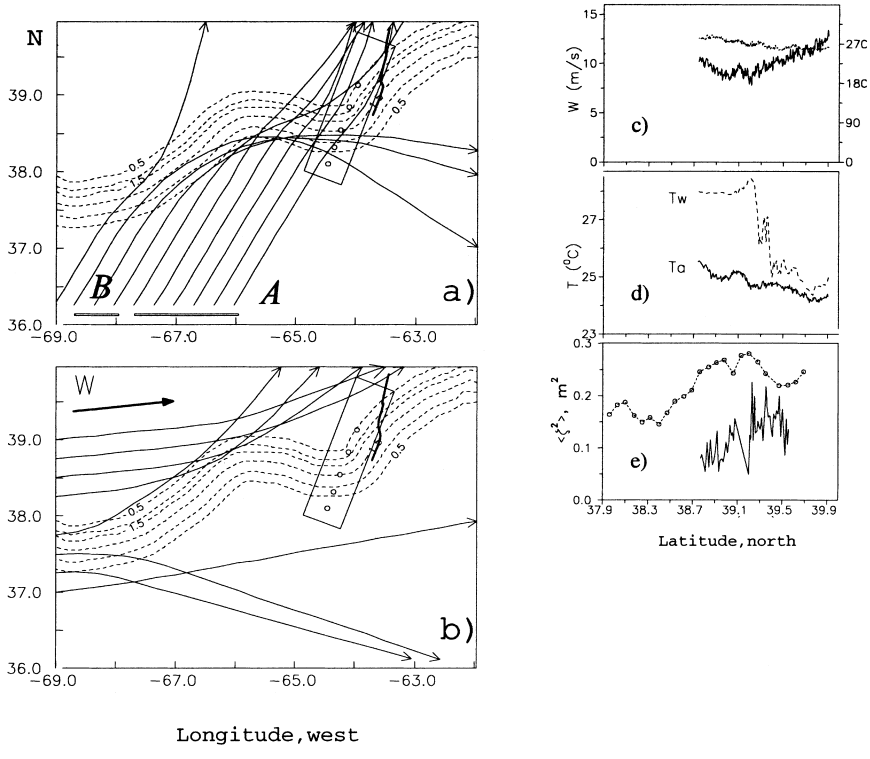

FIGURE 4 On the left. Model surface current field (isolines are drawn in 0.5 m/s). Also shown are: the radar image swath, the locations of spectra presented in Figure 3, and the ship path. (a) wave rays of systems *A* and *B*; (b) wave rays of the wind-driven wave system. On the right. The data of ship measurements along the route #15; (c) Wind speed (solid line) and direction (dotted line); (d) Temperature of water (T_w) and air (T_a); (e) The variance of vertical displacement of the vessel (solid line) and the wave elevation variance retrieved from radar spectra (opened circles).

In a "southern" part of the radar image the trajectories cross, which corresponds to a superposition of waves in image subscene 22 of Figure 3. Only system A penetrates to the northern side of the current, where SAR has registered an unimodal wave field at point 4. The reflection of waves occurs to the west of the area imaged by SAR where the local incidence angle is greater owing to a curve in the jet.

Wave ray calculations presented in Figure 4b explain the absence of a wind wave system on the radar image. Really, the waves oriented along the wind direction are deviated by the current forming a "shadow" area within the image swath. At the same time, locally generated short wind waves would probably not be resolved by radar.

The data of ship measurements along route #15 are also presented in Figure 4 (see Fig. 3 for ship path location). The variance of vertical displacement of the vessel (indirectly reflecting wave elevation variance $\langle\zeta^2\rangle$) grows on the northern side of the current (see Figs. 4e and 4d). Wave variance retrieved from the radar spectra has a similar tendency. The observable changes in wave energy are not connected to the wind (Fig. 4c) and, probably, are a result of wave interaction with a non-uniform current. The growth of wave energy on the northern side of the Gulf Stream is explained qualitatively by local concentration of waves of system A (see Fig. 4a).

Experiment August 29 was carried out at meteorological conditions similar to the previous experiment at a moderate westerly wind of $W = 5\,\mathrm{m/s}$ to $11\,\mathrm{m/s}$ (see Tab. I). The vessel trajectory is shown in Figure 5 on a background of the SST map received from NOAA satellite. The observable thermal structure is less pronounced (in comparison with the previous experiment), which is caused by the influence of continuous and partial cloudiness (C). The Gulf Stream temperature front (T) divides colder shelf water ($T_w = 25°\mathrm{C}$) and rather warm stream waters ($T_w = 28°\mathrm{C}$). Figure 5 shows the SAR image smoothed within the squares $250\,\mathrm{m} \times 250\,\mathrm{m}$. The upper panel of Figure 5 illustrates the general structure of the T_w field with the thermal front marked by a solid line.

The sample of 2-D radar spectra reflects the basic characteristics of wave variability. On the northern periphery of the Gulf Steam two wave systems are observed, to which the spectral maxima A and B correspond. The waves of system A ($\lambda \sim 150\,\mathrm{m}$) propagating in the SE direction are registered on all spectra and cross the current without reflection. Spatial non-uniformity of the wave field is formed basically by system B. Characteristic wavelength of these waves ($80\,\mathrm{m} < \lambda < 110\,\mathrm{m}$) is smaller than that of system A. They were

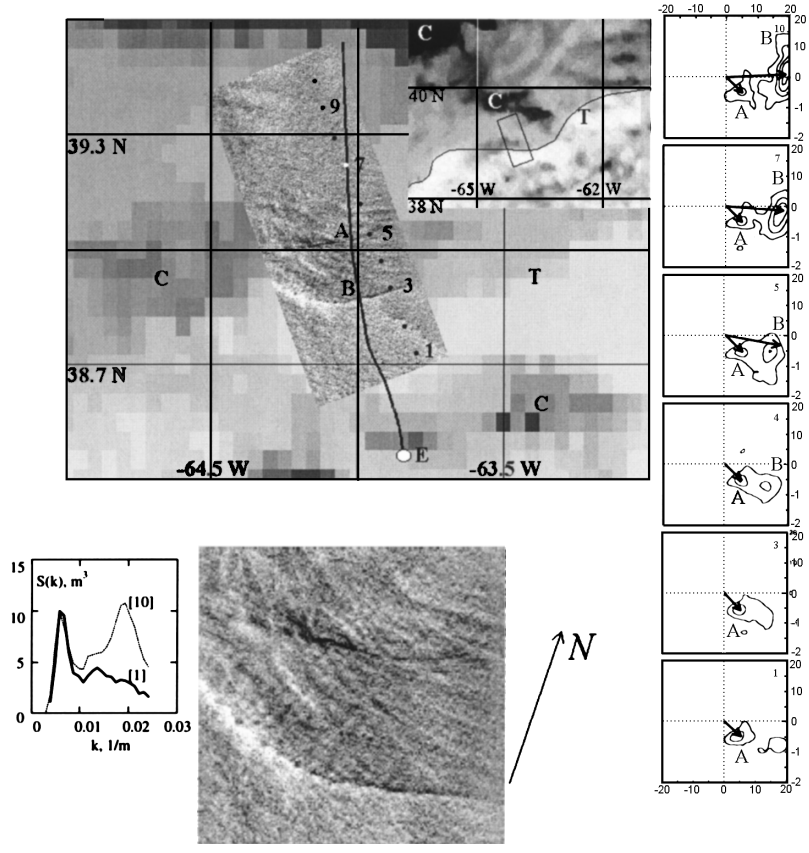

FIGURE 5 On the left. The Gulf Stream ALMAZ-1 SAR image (#2418d, August 29, 1991, 21:45 GMT) on a background of the AVHRR SST (Aug. 29, 06:36 GMT). Also shown are: the vessel route and the numbering of radar image subscenes used for spectra calculation. The upper-right panel displays general view of the thermal front. The lower panels present an enlargement of the linear structures and the wave spectra retrieved from radar image at points #1 and #10. The symbols mark: A and B – linear structures; T – thermal front; C – clouds; E – the site of *in-situ* wave measurements. On the right. The sample of 2-D radar spectra. The symbols A and B mark local maxima corresponding to different wave systems. Isolines are drawn in $0.2\,S_{max}$ where S_{max} is the maximum level in this series of spectra. Discreteness in wavenumber is $\Delta k = 0.005$ rad/m. The arrows show the wavenumbers corresponding to local maxima of model spectra calculated with adiabatic approximation.

registered only on the northern periphery of the Gulf Stream (points 10...4 of Fig. 5) and were not observed in the area of stronger current (points 3...1).

The peculiarities of waves are qualitatively explained by wave packet kinematics on non-uniform current. Figure 6 shows model surface current field and wave rays for system B (panel a) and system A (panel b). Wave rays of system B are calculated for a spatially uniform background wave

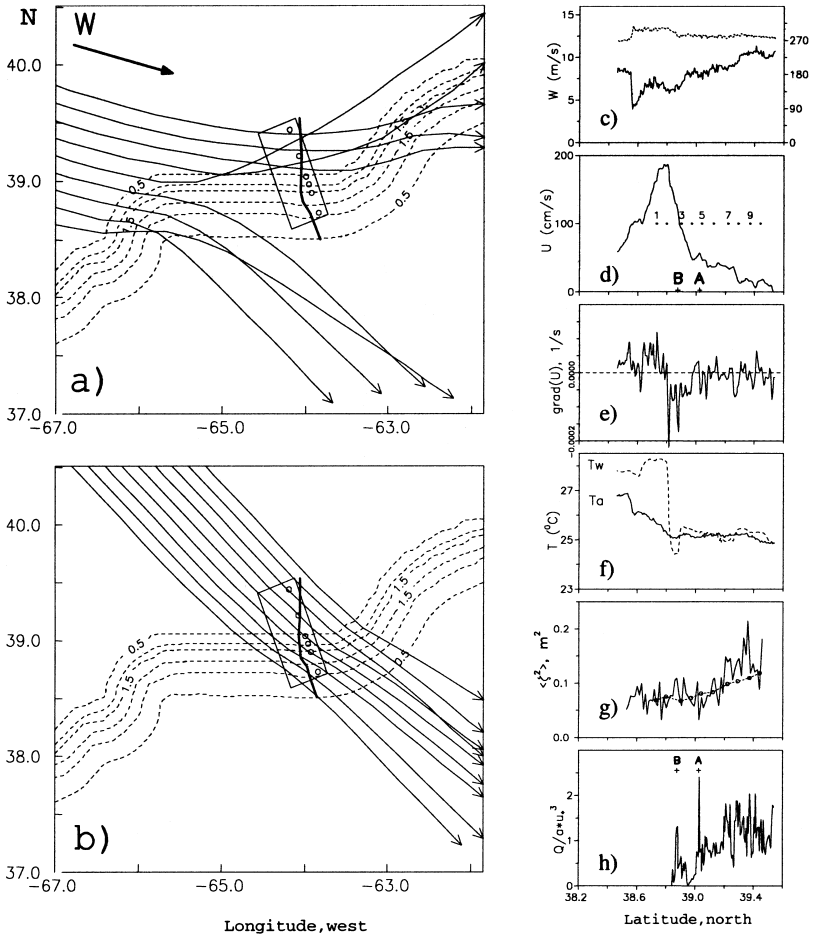

FIGURE 6 On the left. Surface currents for August 29. Isolines of speed are drawn in 0.5 m/s. Also shown are the positions of image subscenes used to calculate spectra presented in Figure 5 and the ship route. (a) Wave rays of system B; the arrow (W) shows wind direction. (b) Wave rays of system A. On the right. Data from R/V VERNADSKY transect (August 29): (c) Wind speed (solid line) and direction (dotted line) ($z = 21$ m). (d) Surface current U, and the positions of radar image subcsenes. (e) Cross current velocity gradient grad U. (g) Sea surface temperature T_w (dashed) and air temperature T_a at $z = 21$ m (solid). (g) The variance of vertical displacement of the vessel (solid) and the wave elevation variance retrieved from radar spectra (opened circles). (h) Wave breaking intensity normalized by friction velocity cubed, Q/au_*^3. Symbols A and B along with crosses show the positions of the linear structures.

field oriented in the along-wind direction. Due to refraction on the anticyclonic meander located at 66°W, the wind-wave system divides into two sub-systems deviating accordingly to the north and to the south of the jet. However, unlike in the previous experiment, only the southern part of the radar image appears in a zone of "shadow" where the energy of the wind waves is much lower than the background. As a result, the wind wave system does not stand out against system A in radar spectra at points 3...1 of Figure 5. Wave rays of system A (see Fig. 6b) expose weaker influence of the current that is caused by smaller incidence angle and greater wavelength as compared to system B.

The concentration of waves on the northern periphery of the Gulf Stream is proved by an increase in the ship's vertical displacement variance and agrees with spatial changes of wave energy inferred from the SAR spectra (see Fig. 6g). The growth of energy is caused by spatial concentration of waves of system B. It is confirmed by the wave spectra $S(k)$ (see Fig. 5) retrieved from the SAR image at points #1 and #10 by applying the empirical MTF presented in Figure 2c.

The Experiment on September 7 was carried out at moderate westerly wind 11 m/s $< W <$ 15 m/s. Unlike the previous days, the T_w field has complex character, caused by instability of the jet. As follows from Figure 7, the radar image covers a zone of an evolving cyclonic Gulf Stream ring. Thus, its northern part appears on a forward front of the warm water's "tongue".

The experimental scheme is shown in Figure 8 as a composition of the SAR image and the SST field for September 4. To estimate possible displacement of the front during the 3 days separating the times of radar and SST surveys, the coordinates of points are put in at which the vessel crossed the thermal front on September 6 and 7. Referring to Figure 8, we find only small changes in the spatial location of the Gulf Stream temperature front that allows use of its configuration recorded on September 4 (see Fig. 7) to analyze data collected on September 7. At the same time, one can expect that the earlier hypothesis of a constant cross current speed profile will not be valid in conditions of a complex configuration of the front, connected with flow instability. Nevertheless, we have performed wave calculations with the model field **U** built using the above assumption.

All radar spectra shown in Figure 8 have local maximum corresponding to waves propagating in the SE direction. They cross the current, keeping practically constant wavelength ($\sim$150 m) and orientation (azimuth $\sim$135°), that agrees with a picture of wave rays (see Fig. 9a), which look

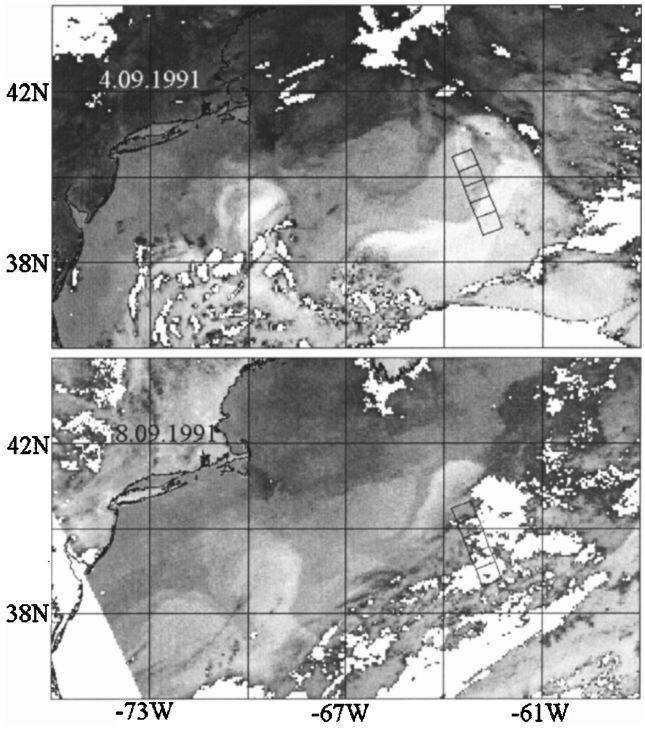

FIGURE 7 AVHRR SST for September 4 and September 8, 1991 with radar image swath (September 7) overlaid.

like quasi-parallel lines on the whole width of the processing area. They result from mutual orientation of waves and current, when the rays penetrate into a jet practically along the front normal, and refraction effects are minimum.

At the same time, the wave energy retrieved from the radar spectra possesses local maximum in the area of maximal current (Figs. 9f and d) that agrees in general with spatial changes in the variance of vertical displacement of the vessel (Fig. 9f). Outside the Gulf Stream and on its northern side (see points 25. . .8 of Fig. 8) the background waves evolving in the SE direction have approximately constant spectral peak level (Fig. 9b). Further, in a southern direction (between points #8 and #1, see Fig. 8) the energy of these waves falls, which is illustrated with the wave spectrum $S(k)$ at point #1 (Fig. 9b). This effect is not explained with a simplified surface current scheme as a flat parallel jet following the configuration of the thermal front.

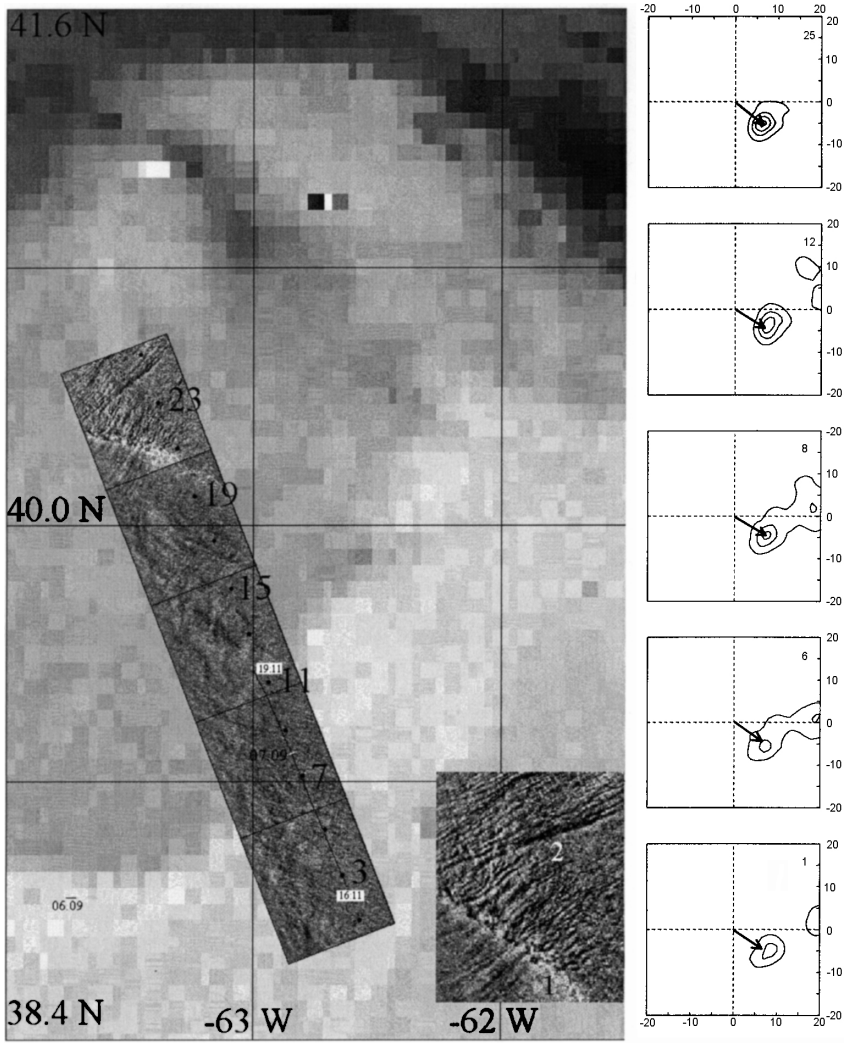

FIGURE 8 On the left. The Gulf Stream ALMAZ-1 SAR image (#2560a, September 7, 1991, 19 : 30 GMT) inlaid in the AVHRR SST field (September 4). Also shown are: the vessel route, the numbering of image subcsenes used for spectra calculations, and the GS front position on September 6 and September 7 according to ship data. The lower panel presents an enlargement of the northern frame of radar image showing (1) – convergence front, (2) – mottled texture. On the right. The sample of 2-D radar image spectra. Isolines are drawn in $0.2S_{\max}$ where $S_{\max}$ is the maximum level in this series of spectra. Discreteness in wavenumber is $\Delta k = 0.005\,\text{rad/m}$. The arrows show wavenumber of the peak of model spectra calculated with adiabatic approximation.

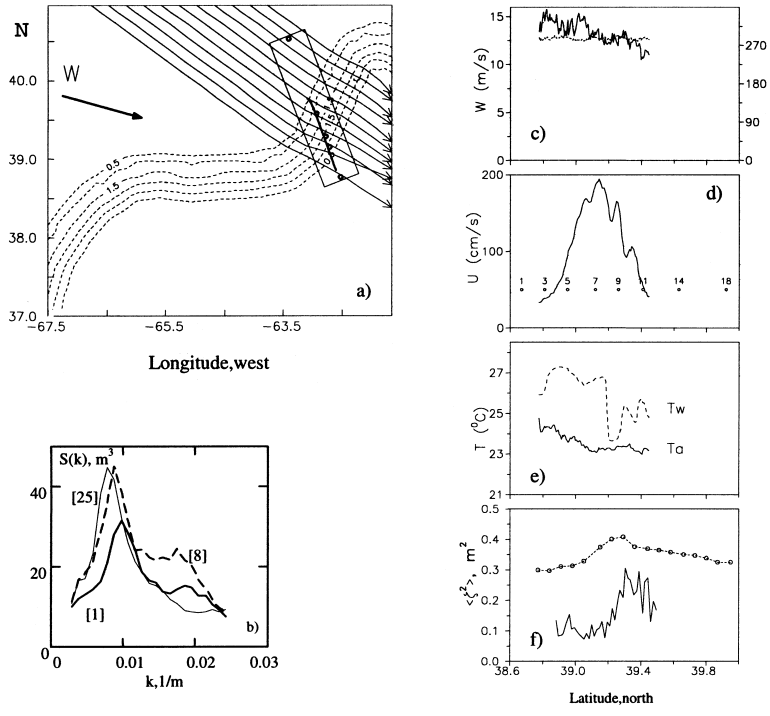

FIGURE 9 On the left. (a) Wave rays overlaid on the surface current (isolines are drawn in 0.5 m/s). Also shown are: the radar image swath, the locations of spectra presented in Figure 8, and the ship route. (b) Wave spectra retrieved from radar image at points #1, #8 and #25. On the right. The data of ship measurements: (c) Wind speed (solid line) and direction (dotted line). (d) Surface current U, and radar image subscenes positions. (f) Temperatures of water (T_w) and air (T_a) at 21 m. (e) The variance of vertical displacement of the vessel (solid line) and the wave elevation variance retrieved from radar spectra (opened circles).

6. RADAR SURFACE CURRENT SIGNATURES

The analysis of the SAR images has allowed us reveal a number of structures connected to the sharp current gradients in the Gulf Stream frontal zone. We were limited to analysis of phenomena of spatial scales of a few kilometers. The specificity of ALMAZ-1 SAR operation (see Section 3) did not allow us to register radar fingerprints of larger scale phenomena, which were observed with ERS-1 SAR (see *e.g.*, Beal *et al.*, 1997).

The Experiment August 28 Figure 3 shows an enlargement of the southern part of the radar image, which reveals a contrast boundary oriented parallel to the temperature front and separating the areas with differing backscatter

level. Note a bright linear structure located to the south of the boundary mentioned above at a distance of ~ 5 km and parallel to it. Similar structures were frequently observed visually and by remote technique at weak and moderate winds in the Gulf Stream area (see *e.g.*, Marmorino *et al.*, 1994; Beal *et al.*, 1997 and literature cited therein) in close vicinity of current convergence lines. Under certain conditions, the waves experience intensification here, cause sea surface roughness increase and radar signal growth.

The Experiment August 29 Let us consider in more detail the observations of linear structures based on data of August 29, when the ship measurements were carried out within the image swath (see Fig. 5). The SAR image presents two strips having negative (A) and varying (B) contrast. They are oriented parallel to the thermal front, and strip B perfectly coincides with its location. The bottom panel of Figure 5 shows an enlarged view of the line features. Within line A the level of radar backscatter is lower than the background one. At the same time, line B possesses varying radar backscatter. Its western part looks as a bright feature, while the eastern part has mostly lower brightness as compared to background one.

For interpretation of these structures, we use the data of ship measurements (Fig. 6) collected during several hours in advance of the satellite survey. Figure 6c illustrates the variability of wind speed and direction. At the moment of imaging, the vessel was at point E (see Fig. 5) where westerly wind of $W = 8$ m/s was observed. Figure 6d presents crosscurrent flow profile, and centers of image subscenes used for radar spectra calculations. Also marked are the points where the vessel crossed the strips A and B, respectively. The strips are located at the northern side of the current profile. Their positions do not correlate unequivocally to spatial variations in cross current velocity shear (Fig. 6e), which have doubled local extremum in close vicinity of line B and no peculiarities corresponding to line A. It indicates on the fact that the origin of the strips is also connected to structure of the cross current circulation, which can't be estimated using EK measuring only one flow component perpendicular to ship's heading. At the crossing by the vessel of strips A and B, slicks and sargassum accumulations were visually observed indirectly indicating current convergence. These data do not yield to quantitative interpretation; however, we can note that the maximum concentration was observed near strip A.

Sargassum accumulations aligned with current boundaries are characteristic of the Gulf Stream frontal zone (Stommel, 1960). That is why, the sea surface brightness may serve as an objective indicator of current

convergence in the Sargasso Sea. As such an indicator we used the measurements of wave breaking intensity Q obtained by TV camera. It can be made, since sargassum as imaged by the camera produces signal spikes similar to those from bright whitecaps, and sargassum accumulations are registered as locally bright objects. In Figure 6h the measurements of Q are normalized with a background dependence $Q_o \sim au_*^3$ (which is proportional to air friction velocity cubed (Wu, 1988)) to exclude variations caused by wind speed and whitecap changes. Sargassum strips are expressed as local maxima in Q/Q_o (see Fig. 6h), and their positions correlate with lines A and B.

The expected fingerprints of the convergence structures are determined by wind speed. At a weak wind, the effect of pollution and surface active material accumulations predominates. That results in slicks with reduced radar backscatter. With wind growth, the surface films are destroyed, and the determining factor becomes concentration of wave energy in convergence zones, that forms bright structures due to roughness increase. The expected radar signature of the current convergence is to be of the same sign as that due to slicks. If convergence acts along with crosscurrent velocity shear, the resulting radar fingerprint can be more complicated.

Lyzenga (1991) has proposed a model of radar contrasts of the ocean fronts based on a local balance approach (Alpers, 1985) for Bragg ripple. If flow parameters vary only in the direction normal to the front, the magnitude and sign of the contrast depends on mutual orientation of radar look direction with respect to the front line, and also on the relation between div**U** and rot**U** (Johannessen *et al.*, 1996). However, the expected contrasts of centimetric wind waves are insignificant. The real radar contrasts of the fronts should be determined by a wider range of wind waves forming the "roughness" of the sea surface (Makin *et al.*, 1995). Thus, the energy of Bragg ripple follows changes of wind resulting from the Marine Atmospheric Boundary Layer reaction to spatial changes in the underlying surface parameters (Kudryavtsev *et al.*, 1997). In a general case, the radar contrasts will depend on wind velocity, radar orientation, the components of current shear tensor, and surface film concentration.

Distinctions in radar signatures of structures A and B are worth noting. Distance between the strips is a few kilometers, so, they were observed (probably) in similar surface wind conditions. The measurements of Q provide estimates of the current convergence in the area of the strips, to probably be stronger for the strip A zone. At the same time, strong crosscurrent shear (see Fig. 6e) is registered near line B, which is absent in vicinity of structure A. Due to line B curving, the waves traveling in the wind

direction experience different changes in surface current in the western and in the eastern parts of line *B*. In the western part, wind waves (directed eastward) cross a current shear zone starting from its southern part toward the northern one, and are influenced by decrease in the current magnitude, which acts to increase wave energy. Conversely, in the eastern part of line *B*, wind-driven waves are influenced by a current increase, which results in wave damping. The above mechanism may be a reason of varying radar signal contrast along line *B*. Thus, it is possible to conclude, that the negative radar contrast of strip *A* is due to slick, and the image of the linear feature *B* is determined by the combined action of floating substances, accumulated in a convergence zone and wave-current shear interaction.

The Experiment September 7 Wind and wave strengthening destroys linear structures, which are not visible on the SAR image collected on September 7 (see Fig. 8). Its basic peculiarity are contrast structures of the "northern" frame located in a zone of the forward front of a warm water "tongue" of the Gulf Stream cyclonic disturbance (see Figs. 7 and 8). Its development is accompanied, probably, by the formation of a convergence zone caused by warm water advection toward the slowly moving shelf water. The local amplification of waves owing to convergence action forms a bright radar signature oriented along the front (1) in the NW–SE direction (see enlargement to Fig. 8). To the north of it, the radar detected wave-like disturbances (2), oriented perpendicularly to the front. Characteristic distance between the strips is a few kilometers. Probably, they result from intensive interaction between warm and cold waters, displaying an unstable current field in an evolving ring accompanied by Internal Wave generation. We shall note that to the south of front where, probably, the currents are small these disturbances are absent. Similar structures in a warm ring of the Gulf Stream (named "mottled texture") were illustrated earlier by Lichy *et al.* (1981) with SEASAT SAR.

7. SUMMARY

Within the framework of the OKEAN-I program the experiments on quasi-synchronous observations of the Gulf Stream frontal zone are performed with ALMAZ-1 SAR and from the R/V AKADEMIK VERNADSKY.

The low orbiting space vehicle, ALMAZ-1, provided rather small values of R/V parameter, therefore the contribution of SAR nonlinear wave

imaging effects were minimum. The comparison of wave parameters obtained by the spectral analysis of SAR images with *in-situ* measurements of waves has shown good conformity. That allows us to determine basic kinematic characteristic: wavelength and wave orientation by radar scene FFT processing. Based on two case observations the wave-radar image MTF is estimated. Its modulus is inversely proportional to wave frequency and decreases with wind speed.

The theory of interaction with jet current (Kenyon, 1971) predicts an opportunity for wave reflection and trapping by a flow. These effects were studied in the third generation model by Holthuijsen and Tolman (1991); however, the real behavior of waves in a zone of large-scale currents requires additional investigations. Using spaceborn SAR, we observed wave reflection by current, which appeared as a combined effect of the current shear and upstream curving of the Gulf Stream. This forms local areas of wave "shadow" and intensification. The concentration of waves at the current boundaries due to a superposition of several systems produces a danger to navigation because of energy increase and significant broadening of the angular spectrum (James, 1974). The operative control of such situations outside of dependence on weather conditions has practical interest and is possible only with the help of SAR.

The convergence strips at the boundaries of water masses are characteristic of the ocean fronts. Here a number of processes forming radar contrasts of different sign take place. Surface films and pollution accumulation suppresses centimetric wind ripples that are responsible for backscattering of radiowaves. Together with this, wave energy is concentrated in convergence zones with possible occurrence of stochastic wave strips *siome* (Uda, 1938; James, 1974). The sea surface roughness growth induced by waves steepening and chaotic breaking increases the radar signal, and after a bright strip occurrence of a dark one is possible. The relative contribution of these two processes depends on the wind speed, surface film characteristics, and current non-uniformity. Probably, at a weak to moderate wind $W < 8\,\mathrm{m/s}$ the film effect is important, and the convergence strip has low radar signal. With wind increase above 10 m/s the sea surface films are destroyed, and the convergence zones get bright radar signature. For a fresh wind (probably stronger than 15 m/s) the efficiency of both mechanisms falls, and the waves, forming the sea surface roughness, are in balance with the local wind.

Comparison of satellite and surface data has shown that linear structures oriented along a thermal front manifested the zones of local maxima in surface current changes. The convergence strip (identified from on board of

the vessel by sargassum accumulations) had low signal on the radar scene received at $W = 8$ m/s. At a distance of several kilometers from it, the area of sargassum enrichment and significant local cross current shift was registered, which displayed as a structure with varying radar signal. The value and sign of radar backscatter variation depends on the mutual orientation of the waves, current gradients, and radar look direction. On a radar image obtained at $W = 12$ m/s the linear structures were not observed. Here the bright area was registered to be coinciding with a probable convergence front caused by warm waters advecting to a zone of slowly moving shelf waters. Also occurring here were the wave-like structures orthogonal to the front. The nature of these "wavy" signatures is not sufficiently clear and requires additional investigations.

Acknowledgments

The field program was realized with financial support from the Fishing Ministry of Russia. This investigation was supported in part by the Grant UD9200 funded jointly by the Ukrainian Government and International Science Foundation. The authors appreciate the contribution of Dr. Pavel Shirokov (Center Almaz, NPO Mashinostroenie), Dr. Gennady Korotaev of Marine Hydrophysical Institute (MHI), Ukranian Academy of Sciences, Dr. Yury Trokhimovsky of Space Research Institute (SRI), Russian Academy of Sciences and Dr. Andrey Smirnov of SRI (now at NOAA ETL) in organization and coordination of the experiment. Dr. Alexandr Babanin of MHI (now at School of Civil Engineering UNSW, Canberra) kindly provided the data of *in-situ* wave records. The data on whitecap coverage were provided by Dr. Vladimir Dulov of MHI. Authors acknowledge valuable comments of Dr. Kristina Katsaros and anonymous reviewer.

References

Alpers, W., Ross, D. B. and Rufenach, C. L. (1981) "On the detectability of ocean surface waves by real and synthetic aperture radar", *J. Geoph. Res.*, **86**(C7), 6481 – 6498.

Alpers, W. R. (1985) "Theory of radar imaging of internal waves", *Nature*, **314**, 245 – 247.

Alpers, W., Bruning, K., Wilde, A., Etkin, V. S., Ts Litovchenko, K., Ivanov, A. Yu. and Zaitsev, V. V. (1994) "Sea wave imaging by the Synthetic Aperture Radars (Comparative analysis of data, received ALMAZ-1 and ERS-1 SAR)", *Sov. J. Rem. Sens.*, **6**, 83 – 95.

Barnett, T. P., Kelley, F. and Holt, B. (1989) "Estimation of the two-dimensional ocean current shear field with a Synthetic aperture radar", *J. Geoph. Res.*, **94**(C11), 16.087 – 16.095.

Beal, R. C., Katz, I. and De Leonibus, P. (Eds.) (1981) "*Spaceborne SAR for oceanography*", The Johns Hopkins University Press, 213 pp.

Beal, R. C., Gerling, T. W., Irvine, D. E., Monaldo, F. M. and Tilley, D. G. (1986) "Spatial variations of ocean wave directional spectra from SEASAT SAR", *J. Geoph. Res.*, **91**(C2), 2433 – 2449.

Beal, R. C., Kudryavtsev, V. N., Thompson, D. R., Grodsky, S. A., Tilley, D. G., Dulov, V. A. and Graber, H. C. (1997) "The influence of the marine atmospheric boundary layer on ERS-1 synthetic aperture radar imagery of the Gulf Stream", *J. Geoph. Res.*, **102**(C3), 5799 – 5814 (in Russian).

Grodskii, S. A., Dulov, V. A. and Kudryavtsev, V. N. (1992) "Observation of surface wave refraction on the Gulf Stream", *Dokl. Akad. Nauk SSSR*, **322**(6), 1162 – 1167.

Grodskii, S. A., Kudryavtsev, V. N., Ivanov, A. Yu., Zaitsev, V. V. and Solov'ev, D. M. (1996a) "Interaction of surface waves with the Gulf Stream according to ALMAZ-1 SAR data", *Issledovanie Zemli iz Kosmosa.*, **3**, 38 – 47 (in Russian).

Grodskii, S. A., Kudryavtsev, V. N. and Ivanov, A. Yu. (1996b) "Study of the Gulf Stream frontal zone using the ALMAZ-1 SAR and *in-situ* ship measurements", *Issledovanie Zemli iz Kosmosa*, **6**, 59 – 70 (in Russian).

Grodsky, S. A., Kudryavtsev, V. N., Ivanov, A. Yu., Zaitsev, V. V. and Solov'ev, D. M. (1996c) "Surface Wave Observation in the Gulf Stream Area Using *ALMAZ-1* SAR". *IGARSS'96*, Lincoln, NB, USA, 27 – 31 May, 1996, **IV**, 1971 – 1973.

Gutshabash, E. Sh. and Lavrenov, I. V. (1986) "Swell transformation on Agulhas current", *Russian Ac. Sci, Izvestija, Atmos. Oceanic Phys.*, **22**(6), 643 – 648.

Hassellmann, K., Raney, R. K., Plant, W. J., Alpers, W., Shuchman, R. A., Lyzenga, D. R., Rufenach, C. L. and Tucker, M. J. (1985) "Theory of Synthetic Aperture Radar Ocean Imaging: A MARSEN View", *J. Geoph. Res.*, **90**(C3), 4659 – 4686.

Holthuijsen, L. H. and Tolman, H. L. (1991) "Effects of the Gulf Stream on ocean waves", *J. Geoph. Res.*, **96**(C17), 12.755 – 12.771.

Irvine, D. E. and Tilley, D. G. (1988) "Ocean wave directional spectra and wave-current interaction from shuttle imaging radar-B synthetic aperture radar", *J. Geoph. Res.*, **93**(C12), 15.389 – 15.401.

James, R. W. (1974) "Dangerous waves along the North Wall of the Gulf Stream", *Mariners Weather Log.*, **18**, 363 – 366.

Johannessen, J. A., Vachon, P. W. and Johannessen, O. M. (1994) "ERS-1 SAR imaging of marine boundary layer processes", *Earth Obs. Quart.*, **46**, 1 – 5.

Johannessen, J. A., Shuchman, R. A., Digranes, G., Lyzenga, D. R., Wackerman, C., Johannessen, O. M. and Vachon, P. W. (1996) "Coastal ocean fronts and eddies imaged with ERS-1 synthetic aperture radar", *J. Geoph. Res.*, **101**(C3), 6651 – 6667.

Kenyon, K. E. (1971) "Wave refraction in ocean currents", *Deep Sea Res.*, **18**, 1023 – 1034.

Kudryavtsev, V. N., Grodsky, S. A., Dulov, V. A. and Bol'shakov, A. N. (1995) "Observation of wind wave field in the Gulf Stream frontal zone", *J. Geoph. Res.*, **100**(C10), 20,715 – 20,727.

Kudryavtsev, V. N., Mastenbroek, C. and Makin, V. K. (1997) "Modulation of wind ripples by long surface waves *via* the air flow: a feed-back mechanism", *Bound. Layer Meteor.*, **83**, 99 – 116.

Lichy, D. E., Mattie, M. G. and Mancicni, L. J. (1981) "Tracking of a warm water ring", In: "*Spaceborne SAR for oceanography*", Eds. Beal, R. C., Katz, I. and De Leonibus, P., 1981, The Johns Hopkins University Press, p. 171 – 184.

Liu, A. K., Peng, C. I. and Schumacher, J. D. (1994) "Wave-current interaction study in the Gulf of Alaska for detection of eddies by syhthetic-aperture radar", *J. Geoph. Res.*, **99**(C5), 10,075 – 10,085.

Lyzenga, D. R. (1991) "Interaction of short surface and electromagnetic waves with ocean fronts", *J. Geoph. Res.*, **96**, 10,765 – 10,772.

Makin, V. K., Kudryavtsev, V. N. and Mastenbroek, C. (1995) "Drag of the sea surface", *Bound. Layer Met.*, **73**, 159 – 182.

Mapp, G. R., Welsh, C. S. and Munday, J. C. (1985) "Wave refraction by warm core rings", *J. Geoph. Res.*, **90**(C4), 7153 – 7162.

Marmorino, G. O., Jansen, R. W., Valenzuela, G. R., Trump, C. L., Lee, J. S. and Kaiser, J. A. C. (1994) "Gulf Stream surface convergence imaged by synthetic aperture radar", *J. Geoph. Res.*, **99**(C9), 18,315 – 18,328.

Mitnik, L. M., Bulatov, N. V. and Lobanov, V. B. (1989) "Ocean synoptic eddies on satellite radar images", *Doklady, Akad. Nauk SSSR*, **307**(2), 454 – 456.

Nilsson, C. S. and Tildesley, P. C. (1995) "Imaging of oceanic features by ERS-1 synthetic aperture radar", *J. Geoph. Res.*, **100**(N C1), 953 – 967.

Sheres, D., Kenyon, K. E., Bernstein, R. L. and Beardsley, R. C. (1985) "Large horizontal surface velocity shears in the ocean obtained from images of refracting swell and *in situ* moored current data", *J. Geoph. Res.*, **90**(C3), 4943 – 4950.

Stommel, G. (1960) "*The Gulf Stream*", University of California Press.

Tilley, D. G. and Beal, R. C. (1994) "ERS-1 and ALMAZ estimates of directional ocean wave spectra conditioned by simultaneous aircraft SAR and buoy measurements", *Atmosphere-Ocean*, **32**(1), 113 – 142.

Uda, M. (1938) "Researches on "siome" or current rip in the seas and oceans", *Geophys. Mag.*, **11**(4), 302 – 372.

Vachon, P. W., Liu, A. K. and Jackson, F. C. (1995) "Near-shore wave evolution observed by airborne SAR during SWADE", *The Global Atmos. Ocean System*, **2**, 363 – 381.

Viter, V. V., Efremov, G. A., Ivanov, A. Yu., Litovchenko, K. Ts., Semenov, S. S., Smirnov, A. I., Trokhimovsky, Yu. G., Shirokov, P. A. and Etkin, V. S. (1993) "Space vehicle ALMAZ-1 - Program OKEAN-1 preliminary results of radar-observations of ocean processes with high resolution", *Issledovanie Zemli iz Kosmosa.*, **6**, 63 – 76 (in Russian).

Wilde, A., Brüning, C., Alpers, W., Etkin, V., Litovchenko, K., Ivanov, A. and Zajtsev, V. (1993) "Comparison of ocean wave imaging by ERS-1 and Almaz-1 synthetic aperture radar", *Proc. Second ERS-1 Symposium*, 11 – 14 Oct., 1993, ESA SP-361 (Jan., 1994), 239 – 245.

Wu, J. (1988) "Variations of whitecap coverage with wind stress and water temperature", *J. Phys. Ocean.*, **18**(10), 1448 – 1453.